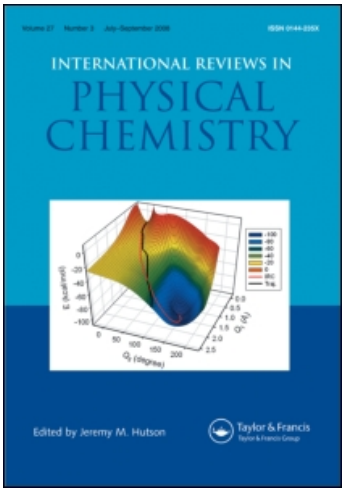

International Reviews in Physical Chemistry
Publication details, including instructions for authors and subscription information:
http://www.informaworld.com/smpp/title~content=t713724383

Energetics and dynamics through time-resolved measurements in mass spectrometry: Aromatic hydrocarbons, polycyclic aromatic hydrocarbons and fullerenes

Chava Lifshitz

Online publication date: 26 November 2010

To cite this Article Lifshitz, Chava(1997) 'Energetics and dynamics through time-resolved measurements in mass spectrometry: Aromatic hydrocarbons, polycyclic aromatic hydrocarbons and fullerenes', International Reviews in Physical Chemistry, 16: 2, 113 — 139
To link to this Article: DOI: 10.1080/014423597230235
URL: http://dx.doi.org/10.1080/014423597230235

INTERNATIONAL REVIEWS IN PHYSICAL CHEMISTRY, 1997, VOL. 16, NO. 2, 113–139

Energetics and dynamics through time-resolved measurements in mass spectrometry: aromatic hydrocarbons, polycyclic aromatic hydrocarbons and fullerenes

by CHAVA LIFSHITZ

Department of Physical Chemistry and The Farkas Center for Light Induced Processes, The Hebrew University of Jerusalem, Jerusalem 91904, Israel

Results of recent work on time-resolved photoionization and electron ionization mass spectrometry carried out in Jerusalem are reviewed. Time-resolved photoionization mass spectrometry in the vacuum ultraviolet is applied to polycyclic aromatic hydrocarbons, for example naphthalene, pyrene and fluoranthene as well as to some bromo derivatives (bromonaphthalene and bromoanthracene). Time-resolved photoionization efficiency curves are modelled by Rice–Ramsperger–Kassel–Marcus QET rate-energy $k(E)$ dependences of the unimolecular dissociative processes and by the rate process infrared radiative relaxation k_{rad}. Experimental results are augmented by time-resolved photodissociation data for the same species, whenever available. Kinetic shifts, conventional and intrinsic (due to competition between dissociative and radiative decay), are evaluated. Activation parameters (activation energies and entropies) are deduced. Thermochemical information is obtained including bond energies and ionic heats of formation. Fullerenes, notably C_{60}, are studied by time-resolved electron ionization and a large intrinsic shift, due to competition with black-body-like radiative decay in the visible is discussed.

1. Introduction

We have witnessed in recent years very significant developments in the basic aspects and in analytical applications of the field of mass spectrometry, particularly in the areas of large species, clusters and biomolecules. While applications have been successful, the physical understanding of many of the phenomena concerning ionization and fragmentation of large molecules is still limited. The mass spectrum of a molecule is the outcome of a series of parallel and consecutive unimolecular reactions. Since the early days of chemical applications of mass spectrometry, there has been an effort to understand the energies and dynamics of the ionic fragmentations, which constitute a mass spectrum. It has been realized that measurements of molecular ionization energies (IEs) and fragment ion appearance energies (AEs) yield invaluable thermochemical information concerning ionic and neutral bond energies and heats of formation [1]. For example, in case of a simple bond cleavage reaction for a relatively small molecule, namely

$$\mathrm{M} \xrightarrow{\mathrm{IE}} \mathrm{M}^+ \xrightarrow{D} \mathrm{F}^+ + \mathrm{N}, \qquad \mathrm{AE} \qquad (1)$$

the ionic bond energy is given by

$$D(\mathrm{F}^+\text{–N}) = \mathrm{AE}(\mathrm{F}^+) - \mathrm{IE}(\mathrm{M}). \qquad (2)$$

It was realized very early that a molecule may have enough energy to dissociate but may not have enough time to do so on the time scale of conventional mass

0144–235X/97 $12·00

spectrometers (about 10 μs). This is particularly so, the larger the molecule, that is the larger its number of vibrational degrees of freedom, leading to slower unimolecular fragmentations. Under these conditions, equation (2) is no longer valid. This holds for many of if not all the large species which are of interest today. A 'kinetic shift' is expected, where the 'kinetic shift' is defined as the excess energy required to produce detectable dissociation of a polyatomic ion in 10^{-5} s [2–4].

Chupka and Berkowitz [5] pointed out in 1960 that the obvious experimental means of evaluating the kinetic shift would consist of measuring the shift of the fragment ionization efficiency curve along the energy axis as the residence time of the ion is varied. This was achieved at first [6, 7] by combining electron ionization with ion trapping in an electron-space-charge negative potential well. Time-resolved ionization efficiency curves and breakdown graphs were measured for benzene [6], chlorobenzene [7], 1,5-hexadiyne [7, 8], pyridine [9], aniline [10], cubane [11], cyclooctatetraene and styrene [12], phenol [13] and iodobenzene [14]. Some of these early measurements have withstood the test of time. For example, the most recent values for the heat of formation of the phenyl radical, $\Delta_f H_0(C_6H_5) = 84{\cdot}3 \pm 0{\cdot}6$ kcal mol^{-1} [15], and its ionization energy, $IE(C_6H_5) = 8{\cdot}0 \pm 0{\cdot}1$ eV [16], combined with the well known values for the heats of formation of $C_6H_6^{\bullet+}$ and $H^{\bullet}$, $\Delta_f H_0(C_6H_6^{\bullet+}) = 237{\cdot}2 \pm 0{\cdot}2$ kcal mol^{-1} and $\Delta_f H_0(H^{\bullet}) = 51{\cdot}63$ kcal mol [1], lead to a calculated critical energy E_0 of $3{\cdot}61 \pm 0{\cdot}13$ eV for the reaction

$$C_6H_6^{\bullet+} \rightarrow C_6H_5^{+} + H^{\bullet}. \quad (3)$$

This compares extremely well with the value obtained in 1974 [6], $E_0 = 3{\cdot}6 \pm 0{\cdot}2$ eV, by applying equation (2) to $AE(C_6H_5^{+})$ measured in an electron ionization–space-charge trapping experiment in which benzene ions were trapped for 900 μs. Another success story has been the time-resolved appearance energy measurements for $C_5H_6^{\bullet+}$ from aniline [10] which demonstrated for the first time, based on the critical energy of reaction (4), that the neutral fragment is HNC rather than HCN:

$$C_6H_5NH_2^{\bullet+} \rightarrow c\text{-}C_5H_6^{\bullet+} + HNC. \quad (4)$$

Formation of HNC rather than the thermodynamically more stable HCN was later shown to be the case [17], by the method of neutral fragment reionization. The electron ionization–electron space–charge trapping experiment suffers from two major drawbacks: firstly poor energy resolution; secondly the breakdown curves which constitute time-resolved breakdown graphs are derived from second derivatives of the electron ionization efficiency curves [8, 9, 18]. The breakdown curve of an ion is the fractional abundance of that ion as a function of the internal energy in the parent and, as such, is a very important attribute; however, the second derivative procedure can lead to large errors.

In 1982 we have introduced for the first time the method of ion tapping in a Paul type cylindrical rf trap in conjunction with photoionization in the vacuum ultraviolet (VUV) [19]. This method has been reviewed recently [20]. It led to improved energy resolution in time-resolved photoionization efficiency (PIE) curves and to time-resolved breakdown curves which were obtained from first derivatives of PIE curves. Most of the systems studied until recently were substituted benzenes. The reason for this choice lies in the high critical energies E_0 for dissociations in these systems and the resultant large kinetic shifts observed. Several of the reaction systems had previously been studied in the microsecond time regime by photoelectron–photoion coincidence (PEPICO) and the adequacy of the proposed models for the microcanonical rate coefficients $k(E)$ was tested using time-resolved photoionization mass spectrometry

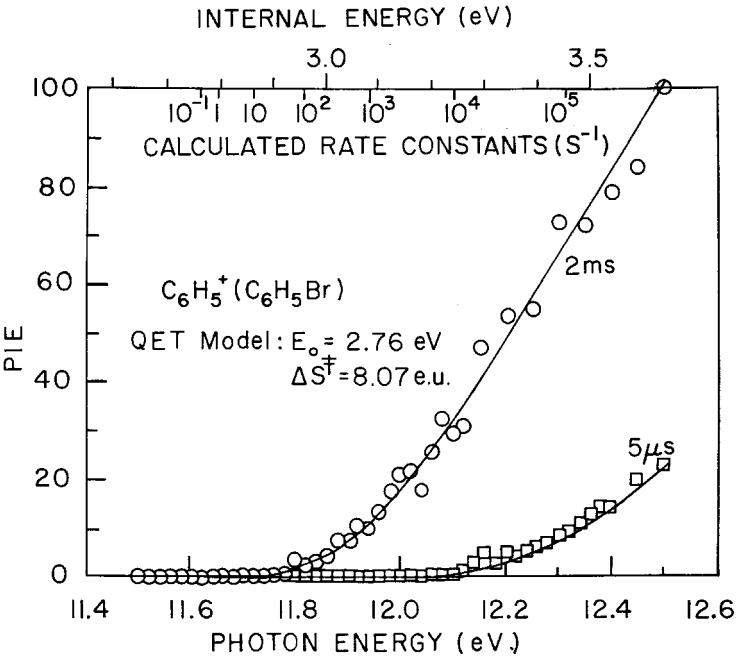

Figure 1. Time-resolved experimental (□, ○) and calculated (——) daughter ($C_6H_5^+$) PIE curves from bromobenzene. The maximum possible internal energy in the ion (upper scale) for a zero-kinetic-energy electron was calculated from the photon energy $h\nu$ (lower scale) and from the known ionization energy of bromobenzene, IE(C_6H_5Br) = 8·97 eV, as follows. The internal energy equals $h\nu - 8{\cdot}97 + 012$ eV, where the 0·12 eV correction is due to the average thermal energy of neutral bromobenzene at the temperature of the experiment (303 K). The calculated bromobenzene ion dissociation rates at these internal energies are also shown on the upper scale. The PIE curves were calculated from a QET model with a critical energy of activation E_0 = 2·76 eV and an activation entropy $\Delta S^{\ddagger}$ = 8·07 eu [22].

(TPIMS) over wider energy and ion lifetime ranges. Reaction systems studied include ethylbenzene [19, 21], cyclooctatetraene [12, 21], bromobenzene [22], iodobenzene [21, 23], phenol [21, 24], pyridine [21], aniline [21], tropone [25], anisole [26], 2,4-hexadiyne [27], 1,5-hexadiyne [28], thiophenol [29], toluene [30–33] and iodotoluene isomers [34].

Experimental time-resolved PIE and breakdown curves were modelled by Rice–Ramsperger–Kassel–Marcus (RRKM) quasiequilibrium theory (QET) calculations. The major outcomes of these studies were the critical activation energy E_0 and the activation entropy $\Delta S^{\ddagger}_{1000\ K}$ for the unimolecular reactions studied, as well as valuable thermochemical information, namely bond energies and ionic and neutral heats of formation. Typical time-resolved experimental and calculated PIE curves obtained during this period are reproduced in figure 1. The predicted shift of the curve along the energy scale [5] is clearly observed, as lower rate constants are being sampled at longer times. Additional modelling was based on *ab-initio* potential energy surface calculations. In the latter case applied to tropylium ion formation from toluene [31–33], the vibrational frequencies and activation energies required for the RRKM QET modelling were obtained from the *ab-initio* calculation. In other cases, notably the C–Br cleavage reaction in bromobenzene,

$$C_6H_5Br^{\bullet+} \rightarrow C_6H_5^+ + Br^{\cdot}, \qquad (5)$$

calculations involving microcanonical variational transition state theory were applied [35]. This procedure was found to be appropriate for locating the transition state in simple bond cleavages, in ionic systems, which possess no reverse activation energy. It has been applied more recently to the benzene reaction (3), leading to a rather high critical energy E_0 = 3·88 eV for that reaction [36].

In recent years the major emphasis of our work has shifted to the larger polycyclic aromatic hydrocarbons (PAHs) and to fullerenes. These species are of interest in combustion and in the chemistry of interstellar space. As larger species were being studied, it became clear that ion trapping can only overcome part of the 'conventional' kinetic shift (CS), that is part of the excess energy required to observe detectable (1%) dissociation within 10 μs [2, 3, 37]. It cannot overcome the 'intrinsic' kinetic shift (IS) which is the energy needed for 10% fragmentation in competition with radiative relaxation of the excited ion [37]. In C_{60} the intrinsic shift is so large that fragmentation cannot be observed using laboratory light sources, limited at the high-energy end by the helium resonance line at 21·21 eV, and we had to resort again to time-resolved electron ionization [38]. In the following we shall discuss some of the recent results obtained for PAHs and their derivatives and for fullerenes by combining ion trapping with VUV photoionization (TPIMS) and with electron ionization. In several instances the TPIMS data were strengthened by a joint study, with the group of R. C. Dunbar at Case Western Reserve University using time-resolved photodissociation (TRPD) and these joint studies [29, 39–41] will be reviewed as well.

2. Experimental details

The experimental technique of TPIMS has been described in detail in [20, 30, 40, 42–46]. Photoionization is induced by a pulsed VUV light source, either the Hinteregger discharge in hydrogen producing the many-line spectrum, or the Hopfield continuum in helium. Photoions are trapped in a cylindrical ion trap (CIT) (figure 2) [47]. They are ejected into a quadrupole mass filter by a draw-out pulse, following a variable delay time. Ions can be stored in the CIT from about 20 μs to 0·5 s. The rf of the potential applied to the cylindrical barrel electrode of the CIT is 0·5 MHz. Ion creation is due to a train of short pulses applied to the light source. An ejection pulse is applied to the end-cap electrode of the CIT nearest the mass filter, and a detection pulse opens the ion counter at the onset of the ejection pulse. The rf voltage is applied to the cylindrical electrode of the CIT throughout the whole cycle. A typical pulsing sequence is represented in figure 3. The effective wavelength resolution employed is 5 Å. This corresponds to energy resolutions of about 0·025 eV near ionization thresholds of 7·5–8·0 eV and of about 0·05 eV and 0·1 eV near fragmentation onsets. A simple Knudsen-type molecular beam source was constructed for low-volatility compounds. Computer control of the mass spectrometer (Extrel; mass range up to m/z = 1200), automatic data acquisition and extended signal averaging are employed.

The experimental method by which a negative electron-space-charge potential well is applied for positive ion trapping has been described in detail recently [38, 48] including the modifications required for converting the ion source of a VG ZAB-2F [49, 50] for ion trapping. This trapping method is particularly useful for experiments employing electron ionization [51–55]. Briefly, ion formation and ion withdrawal are pulsed. The ion formation pulse provides a short (3–6 μs) negative voltage to the filament, which defines the electron energy jump between the filament and the case. The electron energy can be varied between 0 and 70 eV. The ion withdrawal pulse provides a short (2 μs) repeller voltage jump of 10 V to push the ions out for analysis.

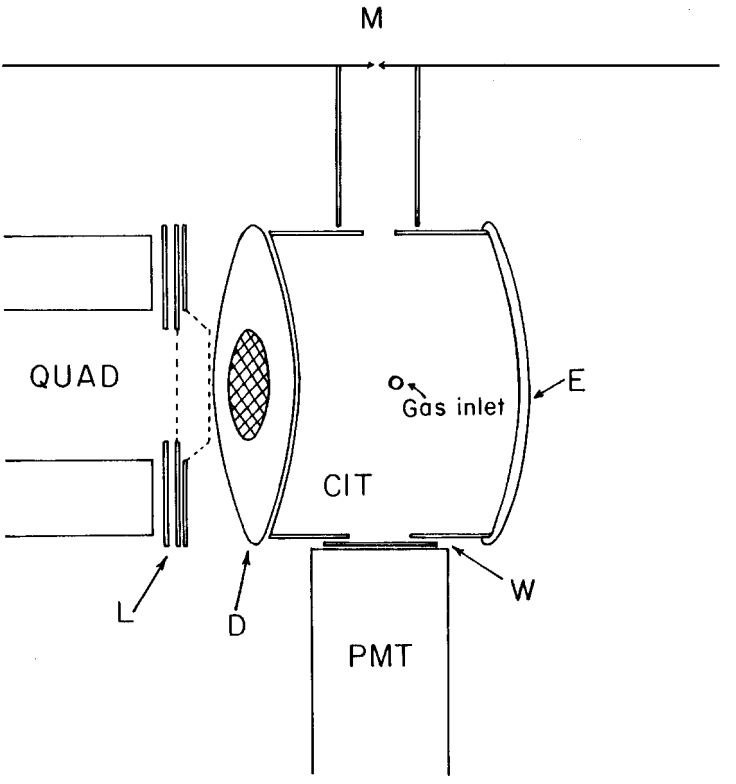

Figure 2. Schematic drawing of the CIT [47] and its connections to the monochromator M, the photomultiplier PMT and the quadrupole mass filter QUAD: E, earthed end-cap electrode; D, draw-out, end-cap electrode; W, sodium-salicylate-coated window; L, ion lens. The cylindrical electrode has a radius r_1 = 2 cm and half-height z_1 = 1·5 cm. Permanent gases or high-vapour-pressure liquids are introduced through the top of the cylindrical electrode [20] while low-volatility compounds are introduced from a Knudsen cell at the bottom.

Ion trapping is achieved through a well focused, relatively high-current electron beam [51]. A trap current of about 10 μA, provided by thermionic emission from a rhenium filament, is employed using a continuous electron beam of about 5 eV which is focused onto the electron collector by ion source magnets providing about 250 G. The pulse sequence employed in the C_{60} experiments [38] was repeated every 250 μs.

3. Results and discussion

3.1. *Time-resolved photoionization efficiency curves*

3.1.1. *Methyl naphthalenes*

1-Methyl and 2-methylnaphthalene radical cations undergo a hydrogen atom loss reaction

$$C_{11}H_{10}^{\bullet+} \rightarrow C_{11}H_9^+ + H^{\bullet} \qquad (6)$$

analogous to the $H^{\bullet}$ loss reaction in toluene [33]. Its thermochemistry was a puzzle for a long time, since AE measurements for $C_{11}H_9^+$ indicated a critical energy higher by about 2 eV than that for the toluene reaction [56–58]. Time-resolved PIE curves for $C_{11}H_9^+$ from 1-methylnaphthalene are represented in figure 4 [43]. Pronounced kinetic shifts (both CS and IS) are observed. Huang and Dunbar [37] were the first to show

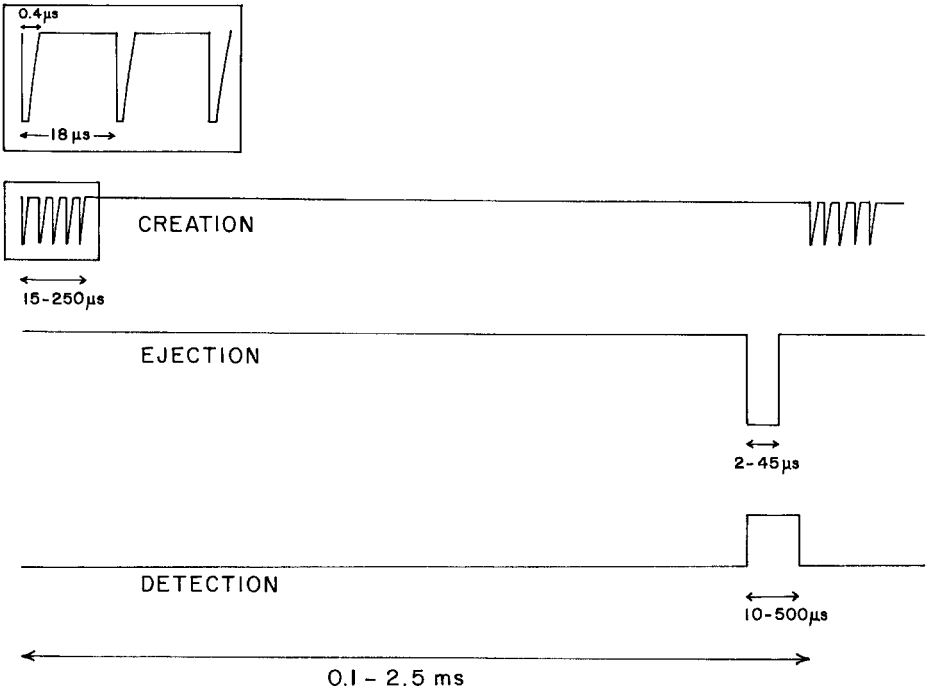

Figure 3. Pulse timing sequence for the operation of the Hopfield continuum in helium in conjunction with ion trapping in the CIT [20].

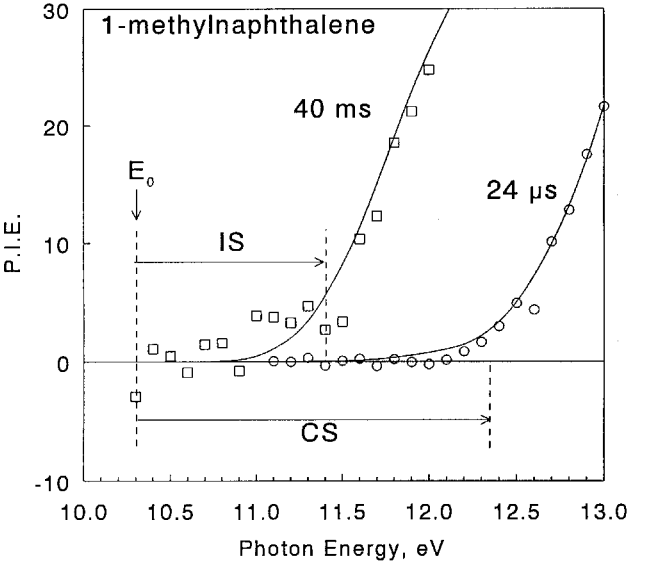

Figure 4. Time-resolved experimental ((○), 24 μs; (□), 40 ms) and calculated (——) daughter ion ($C_{11}H_9^+$) PIE curves for 1-methylnaphthalene. The relative intensities of the experimental PIE curves of the parent served to scale the experimental daughter ion PIEs: CS, conventional kinetic shift; IS, intrinsic kinetic shift [43].

that the $H^{\bullet}$-loss thermochemistries of the toluene and methylnaphthalene systems are similar, but that the larger number of degrees of freedom in methylnaphthalene leads to much larger kinetic shifts. Their conclusion was based on TRPD experiments (to be described in greater detail below) which yielded two microcanonical rate constants $k(E)$ for reaction (6): 70 ± 30 s^{-1} at 3·6 eV internal energy and 530 ± 30 s^{-1} at 4·2 eV. These rate constants were modelled by an RRKM rate–energy curve which led to $E_0 = 2{\cdot}25 \pm 0{\cdot}2$ eV for reaction (6). The PIE curves determined experimentally and modelled theoretically by our group [43] (figure 4) provide a direct manifestation of the predicted kinetic shifts [37].

Time-resolved PIE curves are modelled by RRKM QET calculations as described in detail by Lifshitz and co-workers [20, 22–30]. This is done in the following way. The microcanonical rate coefficient $k(E)$ is calculated as a function of energy by an RRKM program [59]. Time-resolved daughter-ion breakdown curves are calculated from the rate–energy dependence $k(E)$ at 0 K; these give the internal energy dependence of the fractional abundance of the daughter ion. Threshold photoelectron spectra are adopted as the energy deposition functions for the photoionization experiments. The 0 K breakdown curves are convoluted with the instrumental slit function, with the calculated thermal energy distribution at the temperature of the experiment and with the threshold photoelectron spectra. The resultant curves represent the calculated first derivatives of the PIE curves of the daughter ion, provided that the threshold law for photoionization is a step function [3, 60]. These curves are integrated to compare them with the time-resolved experimental PIE curves.

The vibrational frequencies of the reactant ion for methylnaphthalene were adopted [43] in agreement with the Huang–Dunbar [37] model. Those for the transition state were varied slightly from those of Huang and Dunbar to give the best agreement with the experimental PIE curves of figure 4. The rate–energy dependence $k(E)$ is independent of the exact frequency changes made in the transition-state model, as long as the activation entropy $\Delta S^{\ddagger}$ is the same [61]. The activation entropy $\Delta S^{\ddagger} = S(A^{\dagger}) - S(A)$, is calculated from the entropy $S(A)$ of the reactant and the entropy $S(A^{\dagger})$ of the transition state by the well known statistical-mechanics equation

$$S = R \ln Q + RT \frac{d(\ln Q)}{dT}, \tag{7}$$

where Q is the partition function, T the temperature and R the gas constant. A standard temperature at which many neutral and ionic dissociation reactions have been calculated is 1000 K.

The sign and magnitude of $\Delta S^{\ddagger}_{1000\ K}$ are an indication of the degree of tightness or looseness of the transition state. While the transition state for the C–Br bond cleavage in bromobenzene (reaction (5)) is totally loose (orbiting transition state) with $\Delta S^{\ddagger} = +8{\cdot}07$ eu [22] that for $H^{\bullet}$ loss from methylnaphthalene (reaction (6)) is very tight with $\Delta S^{\ddagger} = -15 \pm 5$ eu [37] or $-13{\cdot}3 \pm 1{\cdot}5$ eu [43]. The tightness of the transition state indicates that reaction (6) is not a single-step C–H bond cleavage but, by analogy with the toluene reaction [33], involves rearrangements and formation of benzotropylium in addition to methylnaphthylium ions [37, 43].

The CS and IS were calculated from the rate–energy dependence according to the definitions of the shifts given earlier and are indicated in figure 4. They are in very close agreement with the predictions from TRPD [37]. The IS is appropriate to an ion-trap AE experiment unlimited by ion containment time. In other words, even if we had

Table 1. Kinetic shifts for selected ionic fragmentations.

Reaction	CS[a] (eV)	IS[b] (eV)	References
$C_7H_8^{\bullet+} \rightarrow C_7H_7^+ + H^\bullet$ (toluene)	0·59[b]	0·19[b]	[31, 62]
$C_{11}H_{10}^{\bullet+} \rightarrow C_{11}H_9^+ + H^\bullet$ (methylnaphthalene)	2·05	1·1	[37, 43]
$C_6H_5Br^{\bullet+} \rightarrow C_6H_5^+ + Br^\bullet$ (bromobenzene)	0·3	$\leqslant$ 0·07	[22, 40]
$C_{10}H_7Br^{\bullet+} \rightarrow C_{10}H_7^+ + Br^\bullet$ (1-bromonaphthalene)	1·6	1·1	[40]
$C_{14}H_9Br^{\bullet+} \rightarrow C_{14}H_9^+ + Br^\bullet$ (9-bromoanthracene)	2·9	2·0	[63]
$C_{10}H_8^{\bullet+} \rightarrow C_{10}H_7^+ + H^\bullet$ (naphthalene)	2·4	1·9	[42]
$\rightarrow C_8H_6^{\bullet+} + C_2H_2$	2·2	1·7	
$C_{14}H_{10}^{\bullet+} \rightarrow C_{14}H_9^+ + H^\bullet$ (phenanthrene)	3·5	2·9	[42]
$\rightarrow C_{12}H_8^{\bullet+} + C_2H_2$	4·1	3·3	
$C_{16}H_{10}^{\bullet+} \rightarrow C_{16}H_9^+ + H^\bullet$ (pyrene)	4·5	3·6	[44]
$\rightarrow C_{16}H_8^{\bullet+} + H_2$	6·3	4·7	
$C_{60}^{\bullet+} \rightarrow C_{58}^{\bullet+} + C_2$ (Buckminsterfullerene)	32·5[c]	30·5[c]	[38]

[a] CS, excess energy required to observe 1% dissociation within 10 μs; IS, excess energy needed for 10% fragmentation in competition with radiative relaxation of the excited ion.

[b] Calculated from the known $k(E)$ dependence and from the known radiative decay constant.

[c] Calculated from experimental AEs.

extended the ion trapping time for 1-methylnaphthalene beyond 40 ms we would not have been able to lower AE ($C_{11}H_9^+$) further, because of the IR radiative decay of the parent $C_{11}H_{10}^{\bullet+}$. The kinetic shifts are partly compensated, as expected, by the thermal energy. Table 1 summarizes some kinetic shifts. While the IS and CS for toluene are 0·19 eV and 0·59 eV respectively [31, 62], those for methylnaphthalene are 1·1 ± 0·1 eV and 2·05 ± 0·1 eV respectively [37, 43], demonstrating the strong effect of the molecular size (number of degrees of freedom).

3.1.2. *Bromonaphthalenes*

Hydrogen losses from PAHs constitute major fragmentation reactions under various activation techniques of the isolated ions [64]. It is thus imperative to include them in any kinetic scheme and to know as accurately as possible the C–H bond dissociation energies, and the heats of formation of the fragment ions. A similar problem arose some years ago in connection with the C–H bond cleavage reaction in benzene. This was circumvented by Baer *et al.* [65], Rosenstock *et al.* [66], Dunbar and Honovich [67] through studying the bromobenzene dissociation reaction. While benzene, naphthalene and other PAH radical cations undergo several primary reactions [64, 68, 69], bromobenzene undergoes one simple bond cleavage reaction, forming the phenyl cation and a bromine atom, reaction (5). This reaction, as well as the analogous reactions in chlorobenzene and iodobenzene, led to a fairly well established value for the heat of formation of the phenyl cation, and eventually to the $C_6H_5^+$–$H^\bullet$ bond energy in the benzene radical cation [15, 22, 23, 35, 70–72]. We have adopted a similar approach recently in the case of naphthalene and anthracene, by studying the C–Br bond cleavages

$$C_{10}H_7Br^{\bullet+} \rightarrow C_{10}H_7^+ + Br^\bullet, \quad (8)$$

$$C_{14}H_9Br^{\bullet+} \rightarrow C_{14}H_9^+ + Br^\bullet, \quad (9)$$

in bromonaphthalene and bromoanthracene respectively. The reaction in bromonaphthalene, reaction (8), was studied jointly with the group at Case Western Reserve

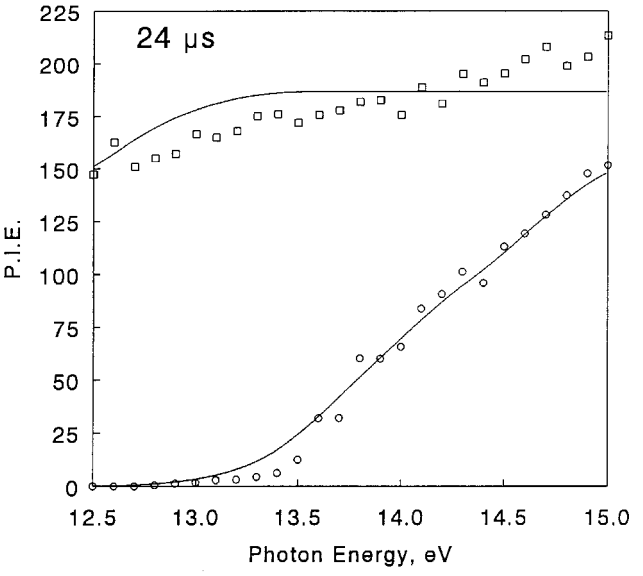

Figure 5. Parent ion, $C_{10}H_7Br^{\bullet+}$ (□), and daughter ion, $C_{10}H_7^+$ (○), PIE curves for 1-bromonaphthalene. The PIE (arbitary units) is plotted against the photon energy at 24 μs: (○), (□), experimental results; ——, calculated [40].

University, using TPIMS and TRPD [40]. A short description of the TRPD experiment follows [29, 73–77]. Parent ions are formed by electron ionization in an ion cyclotron resonance (ICR) cell. They are allowed to undergo thermalization through radiative or collisional cooling for a period of several seconds. The thermalized parent ion population is photoexcited by a 10 ns monochromatic laser pulse. The ensuing photodissociation reaction is followed by monitoring the appearance of daughter ion as a function of time using the detection capabilities of the ICR spectrometer. The abundance of daughter ions is plotted as a function of delay after the laser pulse. Since absorption of a photon gives a parent ion of precisely known internal energy (within the spread of initial thermal energies), each TRPD curve gives a single, well defined point on the rate–energy curve.

The TRPD and TPIMS methods are complementary in a useful way; TRPD gives absolute dissociation rates for ions with well defined internal energies, but it is often restricted to a limited range of internal energies by limitations of available photon wavelengths and photoabsorption cross-sections. TPIMS, on the other hand, is generally convenient over a wide range of ion internal energies, but it yields spectra convoluted over a broad range of ion internal energies which must be deconvoluted by modelling. It has proven useful to use TRPD results to give reliable absolute dissociation rate values, combined with TPIMS results to define the shape of the dissociation rate-energy curve over an extended energy range.

The PIE curves obtained for the parent $C_{10}H_7Br^{\bullet+}$ and daughter $C_{10}H_7^+$ ions from 1-bromonaphthalene at t = 24 μs and 2 ms are represented in figures 5 and 6 respectively. Rate–energy curves, which were in agreement with two $k(E)$ values measured by TRPD for reaction (8) in 1-bromonaphthalene were used to model the experimental PIEs and the resultant calculated PIE curves are included in figures 5 and 6. Several clear changes are observed as a result of the extension of the ion storage time:

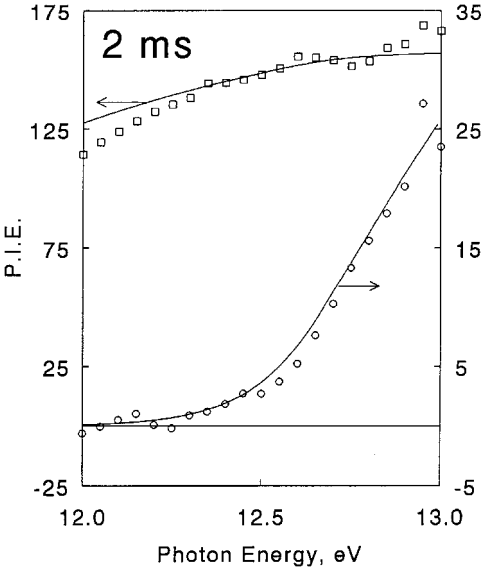

Figure 6. Experimental and calculated PIE curves at t = 2 ms; see caption to figure 5. Note the different scales for the parent (□) and daughter ions (○) [40].

(i) the sharply rising onset for the daughter ion shifts to lower photon energies;
(ii) the abundance of the daughter ion relative to the parent increases;
(iii) the levelling off of the parent ion, which occurs at the daughter ion AE, shifts to lower energies.

Modelling of the TRPD and TPIMS data led to the following activation parameters for 1-bromonaphthalene: E_0 = 3·23 ± 0·07 eV and $\Delta S^{\ddagger}_{1000\ K}$ = 7·7 ± 2·5 eu (table 2). The reactions of both isomers, 1-bromonaphthalene and 2-bromonaphthalene, demonstrate loose transition states characteristic of simple bond cleavages. Kinetic shifts are much higher than for the analogous $Br^{\bullet}$ loss reaction in the bromobenzene ion. The IS and CS are 0·07 eV or less and 0·3 eV respectively for bromobenzene and 1·1 eV and 1·6 eV respectively for 1-bromonaphthalene. It was pointed out [40] that, because of the large kinetic shifts and also the effects of thermal energy, the observed AEs of fragment ions from large ions have little direct quantitative value. Kinetic modelling such as that carried out for bromonaphthalene is essential for deriving useful thermochemical values from fragmentation data. Equating E_0 with the C–Br bond energy, the heat of formation of the α-naphthyl cation was deduced to be [40] $\Delta_f H^0_0(C_{10}H^+_7)$ = 281 ± 3 kcal mol^{-1}. Other aspects of the thermochemistry will be discussed in a later section.

3.1.3. *Pyrene and fluoranthene*

Pyrene and fluoranthene are isomeric $C_{16}H_{10}$ PAHs. It has been pointed out that isomeric PAHs give almost identical fragmentation patterns since they can accommodate a large amount of internal energy before undergoing fragmentation, and isomerization processes are very likely to occur [64]. The pyrene–fluoranthene isomer pair was studied to determine the C–H bond energies, the heats of formation of the product ions, the kinetic shifts (IS and CS), and the activation parameters of the parallel and consecutive $2H^{\bullet}$ and H_2 losses, and to find out whether isomerization takes place prior to fragmentation.

Table 2. Activation parameters for selected ionic fragmentations.

Reaction	E_0 [a] (eV)	$\Delta S^{\ddagger}_{1000\ K}$ [b] (eu)	Reference
$C_7H_8^{\bullet+} \rightarrow C_7H_7^+ + H^{\bullet}$ (toluene)	2·11	− 11·7	[62]
$C_{11}H_{10}^{\bullet+} \rightarrow C_{11}H_9^+ + H^{\bullet}$ (methylnaphthalene)	2·41 ± 0·02	− 13·3 ± 1·5	[43]
$C_6H_5Br^{\bullet+} \rightarrow C_6H_5^+ + Br^{\bullet}$ (bromobenzene)	2·76	+ 8·07	[22]
$C_{10}H_7Br^{\bullet+} \rightarrow C_{10}H_7^+ + Br^{\bullet}$ (1-bromonaphthalene)	3·23 ± 0·07	+ 7·7 ± 2·5	[40]
$C_{14}H_9Br^{\bullet+} \rightarrow C_{14}H_9^+ + Br^{\bullet}$ (9-bromoanthracene)	3·30 ± 0·08	+ 6·5 ± 1·0	[63]
$C_6H_6^{\bullet+} \rightarrow C_6H_5^+ + H^{\bullet}$ (benzene)	3·66; 3·88	+ 2·7	[61, 78]; [36]
$\rightarrow C_6H_4^{\bullet+} + H_2$	3·69	− 0·5	
$\rightarrow C_4H_4^{\bullet+} + C_2H_2$	4·16	+ 10·6	
$C_{10}H_8^{\bullet+} \rightarrow C_{10}H_7^+ + H^{\bullet}$ (Naphthalene)	4·48 ± 0·10	+ 5·6 ± 2	[41]
$\rightarrow C_8H_6^{\bullet+} + C_2H_2$	4·41 ± 0·20	+ 3·5 ± 3	
$C_{16}H_{10}^{\bullet+} \rightarrow C_{16}H_9^+ + H^{\bullet}$ (pyrene)	4·60 ± 0·04	+ 10·7 ± 2	[44, 45]
$\rightarrow C_{16}H_8^{\bullet+} + H_2$	3·52 ± 0·15	− 12·7 ± 2	
$C_{16}H_{10}^{\bullet+} \rightarrow C_{16}H_9^+ + H^{\bullet}$ (fluoranthene)	4·38 ± 0·04	+ 12·1 ± 2	[45]
$\rightarrow C_{16}H_8^{\bullet+} + H_2$	3·34 ± 0·15	− 13·6 ± 2	
$C_{60}^{\bullet+} \rightarrow C_{58}^{\bullet+} + C_2$ (Buckminsterfullerene)	7·1 ± 0·4; ⩽ 7·6	− 0·8; + 4·4	[79–82]

[a] Critical energy of activation.
[b] Activation entropy.

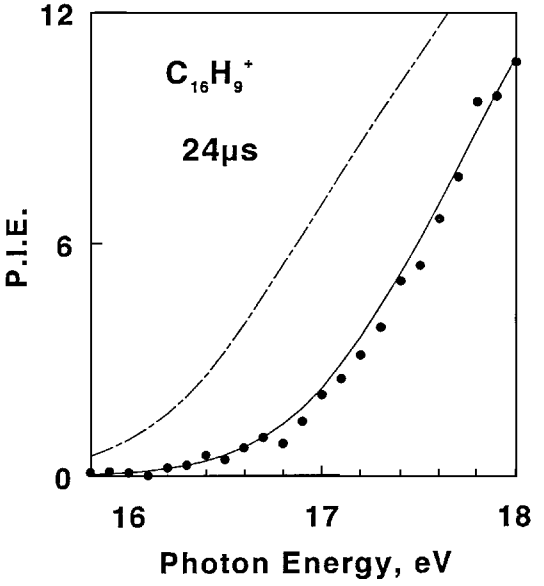

Figure 7. Experimental (●) and calculated (——, ——·——) PIE curves for $C_{16}H_9^+$ from fluoranthene in the microsecond range: (——) direct dissociation model; (——·——), isomerization model [45].

Both reaction systems demonstrate [44, 45] two consecutive $H^{\bullet}$ losses, as well as a parallel H_2 elimination,

$$C_{16}H_{10}^{\bullet+} \rightarrow C_{16}H_8^{\bullet+} + H_2, \quad (10)$$

$$C_{16}H_{10}^{\bullet+} \rightarrow C_{16}H_9^{+} + H^{\bullet}, \quad (11)$$

$$C_{16}H_9^{+} \rightarrow C_{16}H_8^{\bullet+} + H^{\bullet}. \quad (12)$$

The fluoranthene radical cation is less stable than the pyrene radical cation. The fluoranthene PIE data were modelled in two alternative ways: direct dissociation; isomerization to pyrene prior to dissociation. The experimental and calculated PIE curves for $C_{16}H_9^+$ from fluoranthene are represented in figure 7. In the direct dissociation model the parameters for the three reactions were changed until a fit was obtained with time-resolved experiments for all three reactions. Under these circumstances, the dissociations of fluoranthene are independent of those of pyrene and the observation of a similar set of reactions (10)–(12) is fortuitous and reflects only the relative stability of the reaction products, whose structures are totally different from those formed by the same set of formal reactions from pyrene. A schematic potential energy profile for the pyrene–fluoranthene system is shown in figure 8. Independent dissociations of the two isomeric systems would indicate an isomerization barrier which is higher than the respective dissociation limits. If the isomerization barrier is low, then the dissociation rates should be identical at similar absolute internal energies [83, 84]. The internal energy of the dissociating fluoranthene radical cation is higher, at the same total energy, if isomerization precedes dissociation, owing to the difference in the heats of formation of the two isomeric ions.

Modelling of the experimental results was possible only by assuming no isomerization of fluoranthene$^{\bullet+}$ to pyrene$^{\bullet+}$ (see figure 7). The C–H bond energy in

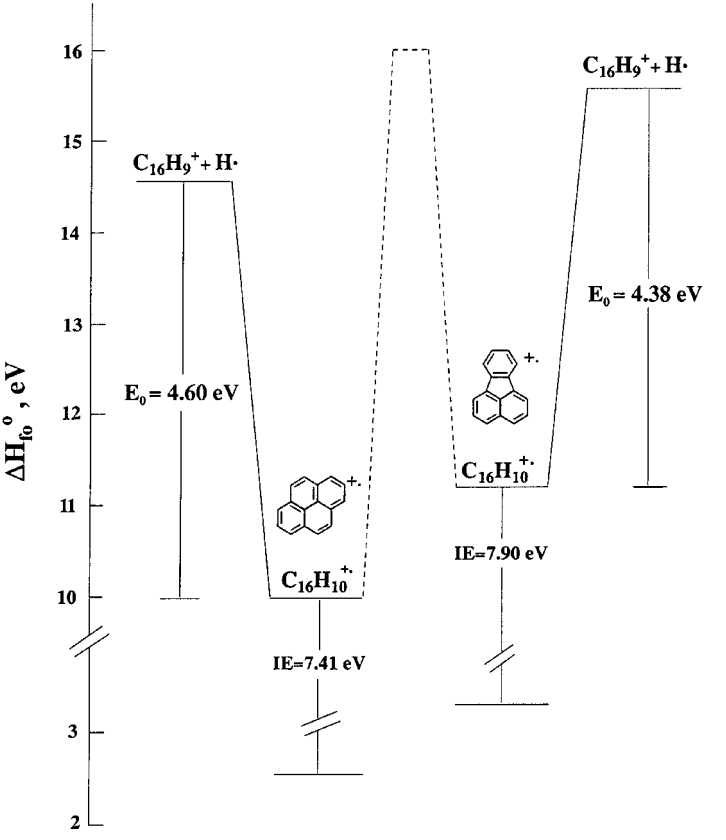

Figure 8. Schematic potential energy profile for pyrene$^{\cdot+}$ and fluoranthene$^{\cdot+}$ isomerizations and dissociations (reactions (11), only) [45].

fluoranthene$^{\cdot+}$ is lower (4·38 eV) than in pyrene (4·60 eV) and a different (less stable) $C_{16}H_9^+$ isomer is produced. It would be interesting to validate these conclusions by other means (different experiments and possibly high-level *ab-initio* calculations). At any rate, the TPIMS data do not support the notion that isomerization necessarily precedes dissociation in all PAH radical cations. Further isomeric pair systems are currently being studied (e.g. anthracene–phenanthrene) [85].

3.2. *Rate–energy dependences*

The microcanonical rate constant $k(E)$ dependence upon the internal energy of the ion is a most basic attribute of the unimolecular fragmentation of a polyatomic ion. TPIMS only provides such data in an indirect way by modelling time-resolved PIE curves as explained above. The bulk of the information on rate–energy dependences for ionic systems was obtained through coincidence experiments, notably PEPICO due to Baer and co-workers [83, 84, 86]. However, while these $k(E)$ measurements were very informative they were limited to the microsecond time regime, that is to $10^4\ s^{-1} < k(E) < 10^7\ s^{-1}$. The TRPD method and its combination with TPIMS allowed for the first time the determination of the rate constants in the range $10^1\ s^{-1} < k(E) < 10^4\ s^{-1}$. This range of rate–energy dependences is crucial for large polyatomic ions and for the study of the competition between dissociative and radiative decay.

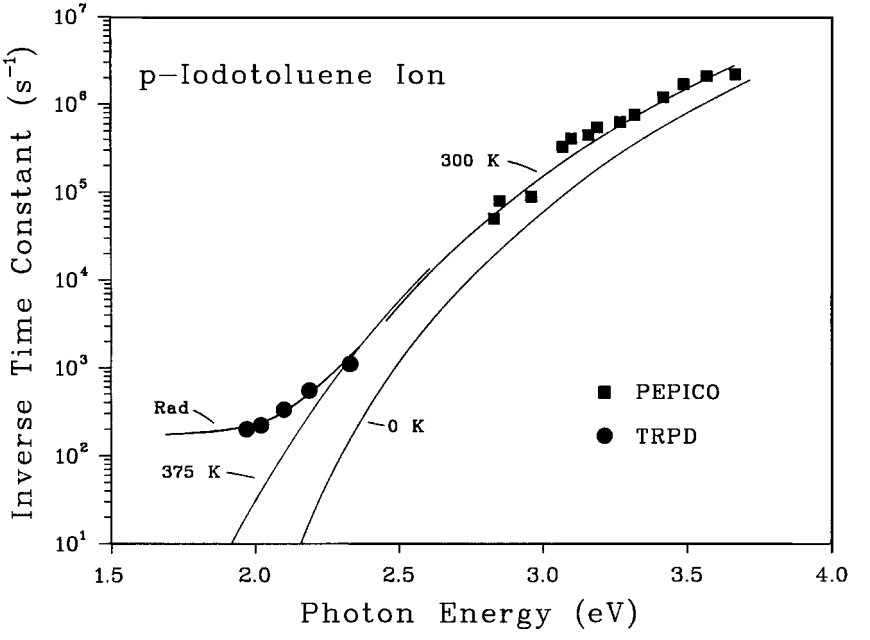

Figure 9. Inverse time constants (●) for the TRPD ion-appearance curves for reaction (13) in *p*-iodotoluene, together with the dissociation rates (■) reported by Olesik *et al.* [86] from PEPICO dissociation data. The 0 K rate–energy curve is the RRKM model calculation with E_0 = 1·9 eV and $\Delta S^{\ddagger}_{1000\ K} = -4$ eu. The PEPICO experiment had a characteristic temperature of 300 K while the TRPD experiment was for 375 K. The curves at 300 and 375 K were calculated by adopting the corresponding thermal spreads of ion internal energies. The curve labelled Rad was calculated using a 375 K thermal distribution and adding the effect of infrared radiative relaxation [39].

3.2.1. *p-Iodotoluene*

The slow time-resolved photodissociation of *p*-iodotoluene$^{\bullet+}$ was studied by Dunbar and Lifshitz [39]. At energies within a few electronvolts of threshold, the only dissociation observed is loss of iodine:

$$CH_3C_6H_4I^{\bullet+} \rightarrow C_7H_7^+ + I^{\bullet}. \qquad (13)$$

At the time of the study this was the slowest dissociation which had been time resolved for ions of well defined internal energies.

Inverse time constants for fragment ion appearance ranging from 2×10^2 to $1{\cdot}1 \times 10^3$ s^{-1} were obtained. These numbers were specified as inverse time constants rather than rate constants since, in the presence of radiative relaxation, the time constant of the ion appearance curve does not correspond to the dissociation rate constant. The inverse ion-appearance time constants are plotted as a function of photon energy in figure 9. It was clear [39] that with increasing wavelength (decreasing photodissociation energy) the dissociation rate dropped off sharply but levelled off at longer wavelengths, trending towards a limiting inverse time constant of around 150 s^{-1}. This levelling off was attributed to the onset of competition from radiative relaxation of the photoexcited parent ion. Further quantitative understanding of the dissociation rates, and construction of the true rate–energy curve from the observed results (figure 9), depended on modelling of the kinetics of the system. The slow TRPD

results were combined with the earlier PEPICO results in the faster dissociation regime [86] to arrive at a complete picture of the dissociation behaviour and the rate–energy curve of the ion. The infrared (IR) relaxation of the photoexcited ion was calculated by kinetic modelling to give an energy loss rate of 6·2 eV s^{-1} corresponding to a rate process radiative relaxation with k_{rad} = 160 s^{-1}. The dissociation kinetics of the ion were in accord with an RRKM model with E_0 = 1·9 eV and $\Delta S^{\ddagger}_{1000\ K} = -4$ eu. Electron-space-charge trapping experiments from our group [34] as well as repeated TRPD experiments [87] from Dunbar's group demonstrated that iodotoluene isomers undergo a two-channel dissociation forming: channel I, the tolyl ion; channel II, the benzyl and/or tropylium ions. The branching ratio between the two channels I and II is energy (and time) dependent with *p*-iodotoluene$^{\bullet+}$ reacting mostly via channel II with E_0 = 1·89 eV and $\Delta S^{\ddagger} = -6{\cdot}98$ eu [87]. Kinetic shifts were derived [39] on the basis of the 0 K $k(E)$ curve (figure 9) of the RRKM model and of the limiting radiative decay constant of 160 s^{-1} to be IS = 0·3 eV and CS = 0·6 eV.

3.2.2. *Naphthalene*

Leach and co-workers [69, 88, 89] have studied naphthalene and perdeuteronaphthalene by threshold photoelectron–photoion coincidence (TPEPICO) and by RRKM QET calculations. Naphthalene$^{\bullet+}$ undergoes several parallel reactions, the major reactions being H$^{\bullet}$ loss and acetylene elimination:

$$C_{10}H_8^{\bullet+} \rightarrow C_{10}H_7^{+} + H^{\bullet}, \tag{14}$$

$$C_{10}H_8^{\bullet+} \rightarrow C_8H_6^{\bullet+} + C_2H_2. \tag{15}$$

The TPEPICO method was applied to reaction (15) in naphthalene-d_8 by Rühl *et al.* [69]. Dissociation rates for the C_2D_2 loss channel were measured between 16 and 17·7 eV photon energies (corresponding to internal energies of between 8·3 and 9·7 eV) and fitted by RRKM QET calculations, resulting in a critical energy of activation E_0 = 3·50 eV and an activation entropy, $\Delta S^{\ddagger} = -3{\cdot}4$ eu. The naphthalene reaction system was studied by the TPIMS method [42] and time-resolved PIE curves were modelled by RRKM QET giving a very different set of activation parameters for reaction (15) in naphthalene-d_8, namely E_0 = 4·60 eV and $\Delta S^{\ddagger}_{1000\ K} = +5{\cdot}6$ eu. Figure 10 reproduces the rate–energy dependences for the two models and includes the coincidence rate constants measured by Rühl *et al.* [69]. The model based on the TPIMS data fitted the experimental coincidence data almost as well as the original model and had the added advantage that the E_0 = 4·6 eV value agreed precisely with the calculated endothermicity provided that $C_8H_6^{\bullet+}$ was phenylacetylene$^{\bullet+}$, the most stable isomer known at that time [1, 42]. Inspection of figure 10 led to the conclusion that at least one microcanonical rate constant should be measured at a lower internal energy, so that a decision could be made between the two models. This has been done by TRPD for both $C_{10}H_8^{\bullet+}$ and $C_{10}D_8^{\bullet+}$ at internal energies of 7·10 and 7·13 eV respectively. Branching ratios between H$^{\bullet}$, H_2 and C_2H_2 losses were determined, so that individual rate constants were determined as well for all three reaction channels in the two isotopomers [41]. The RRKM model which fitted the TRPD data as well as the previous experimental data and was in agreement with several further constraints [41] gave for reaction (15) in naphthalene-d_8 the activation parameters E_0 = 4·41 ± 0·20 eV and $\Delta S^{\ddagger}_{1000\ K}$ = 4·7 ± 3 eu, in fairly good agreement with the TPIMS model. Recent *ab-initio* calculations [90] have indicated that the $C_8H_6^{\bullet+}$ ion which is

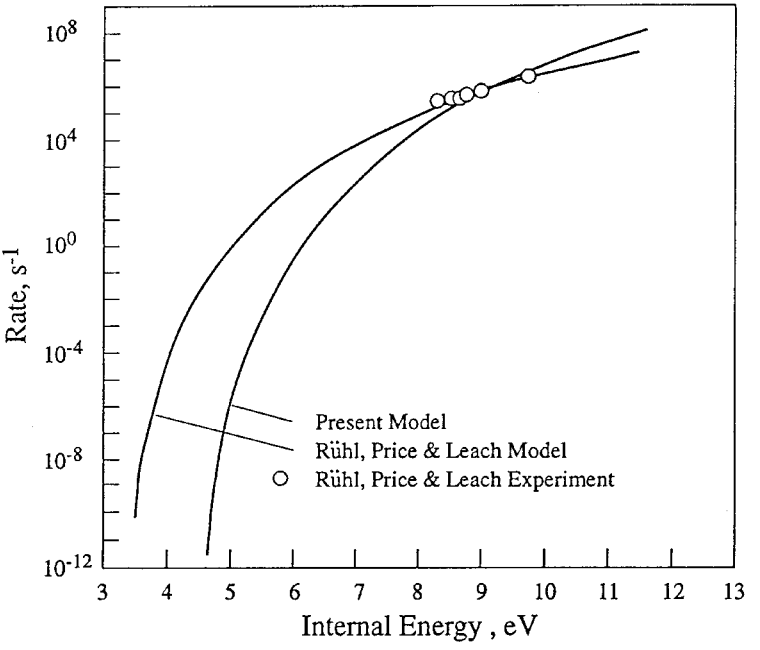

Figure 10. Comparison of the RRKM model based on time-resolved PIE curves (labelled Present Model) with that of [69] and the experimental results based on PEPICO [69] for the $k(E)$ dependence on energy for reaction (15) in naphthalene-d_8 [42].

formed from naphthalene is actually benzocyclobutadiene$^{\bullet+}$ which is slightly more stable than phenylacetylene$^{\bullet+}$. A similar result has been obtained by our group for C_2H_2 elimination from anthracene$^{\bullet+}$ using density functional theory calculations [91]. These results led to the suggestion [90] that a new class of positive ions composed of polyaromatic frames adjacent to cyclobutadiene rings may be present in interstellar space. Formation of the cyclobutadiene ring system in naphthalene, but not in benzene, may be the reason for the lower $\Delta S^{\dagger}$ value (table 2) for the acetylene elimination from napthalene$^{\bullet+}$.

The re-evaluation of the C–H bond strength of the naphthalene ion was a major additional result of the TRPD experiment [41], besides settling the open question concerning the $k(E)$ model for acetylene elimination. The rate–energy dependences for reactions (14) and (15) are represented in figure 11. The RRKM model which fits best the experimental data gives for reaction (14), the H$^{\bullet}$ loss from naphthalene, E_0 = 4·48 ± 0·10 eV and $\Delta S^{\ddagger}_{1000\ K}$ = 5·6 ± 2 eu. Two results become evident (table 2).

(1) The critical energies for H$^{\bullet}$ loss and C_2H_2 elimination are nearly equal. This is in agreement with the experimental observations that branching ratios are not greatly different from unity for C_2H_2 loss relative to H$^{\bullet}$ loss [41].

(2) The critical energy for H$^{\bullet}$ loss from naphthalene$^{\bullet+}$ is at least 0·6 eV higher than that for H$^{\bullet}$ loss from benzene$^{\bullet+}$. Since the H$^{\bullet}$ loss has a relatively high positive activation entropy, it is clearly a loose transition state reaction, with no reverse activation energy, and E_0 can be equated with the C–H bond energy. In other words, the C–H bond energy of the naphthalene$^{\bullet+}$ is 4·48 eV.

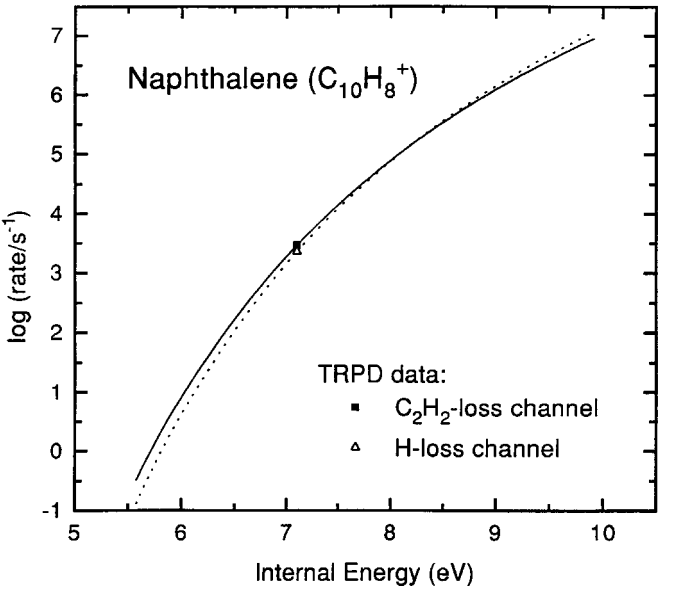

Figure 11. TRPD experimental values for the rate constants of equation 14 (△, -----) and equation 15 (■, ——). The curves are the RRKM rate–energy curves corresponding to the model of [41] and table 2. Note that these curves in addition to passing through the TRPD points, are strongly constrained to agree with the TPIMS results, as well as being constrained by other considerations detailed in [41].

3.3. *Time-resolved breakdown curves*

The breakdown curve of an ion gives its fractional abundance as a function of energy. A collection of breakdown curves of all the ions from a certain molecule constitutes the breakdown graph of a molecule. For a single unimolecular reaction the fractional abundance of the parent at time t is given by $\exp[-k(E)t]$ and that of the daughter by $1-\exp[-k(E)t]$ and their breakdown curves are clearly time dependent and calculable from rate-energy dependences.

Time-resolved breakdown curves were calculated for the first time for $Cl^{\bullet}$ loss from the chlorobenzene radical cation and were compared with experimental electron ionization data by Lifshitz *et al.* [7]. The idea of employing time-resolved breakdown graphs for kinetic shift determinations has been adopted by Rosenstock and co-workers [66, 70, 92–94]. Experimental data obtained by the variable-time PEPICO technique were analysed by QET calculations. Rosenstock and co-workers coined two terms, namely the cross-over energy which is the energy at the 50% point in the long-time parent-fragment curves and the cross-over shift which is the energy difference between the cross-over points of the breakdown curves obtained at two different times. Variable-time PEPICO has produced time-resolved breakdown curves directly, without limiting assumptions, and with high-energy resolution, over a limited time range of microseconds [4].

3.3.1. *Anisole*

TPIMS does not furnish time-resolved breakdown curves directly. These can be obtained from normalized first-derivative time-resolved PIE curves of the parent and daughter ions. In some of our earlier work, for example on formaldehyde elimination from anisole [26],

$$C_6H_5OCH_3^{\bullet+} \rightarrow C_6H_6^{\bullet+} + CH_2O, \qquad (16)$$

we have adopted this approach (figure 12). This was followed by a sensitivity analysis of the calculated breakdown curves, via the cross-over energy and cross-over shift, to the activation parameters: the activation energy and activation entropy. This approach has been abandoned in recent years and, as explained earlier, calculated time-resolved breakdown curves are integrated to compare them with experimental PIE curves, instead of comparing derivatives of PIE curves with the calculated breakdown curves.

3.3.2. *Bromonaphthalene*

A recently calculated set of time-resolved breakdown curves for reaction (8) in bromonaphthalene [40] is represented in figure 13. In these calculated curves we have employed: RRKM dissociative rate constants (which fitted the TPIMS PIE data of figures 5 and 6 and the two rate constants determined experimentally by TRPD [40]), as well as an energy-independent rate constant for radiative decay in the infrared region, $k_{rad} \simeq 500\ s^{-1}$. In earlier work on bromobenzene [22] we have calculated energy-dependent radiative rate constants according to Dunbar [95]. The procedure requires knowledge of the IR absorption intensities of the molecule, in order to calculate the intrinsic oscillator strength of each active normal-mode quantum state. The rate–energy dependence of k_{rad} is rather flat and the choice of an energy-independent rate in modelling calculations seems justified. Many of these radiative decay rate values are known from the work of Dunbar and co-workers on radiative cooling of polyatomic ions. For example, the radiative decay rate of the naphthalene ion is of the order of $10^2\ s^{-1}$ [96–98]. A more detailed study of IR radiative decay in naphthalene$^{\bullet+}$ has appeared recently [99].

3.3.3. *Buckminsterfullerene C_{60}*

Lifshitz and co-workers [100] have calculated time-resolved breakdown graphs and kinetic shifts for the C_2 evaporation from $C_{60}^{\bullet+}$:

$$C_{60}^{\bullet+} \rightarrow C_{58}^{\bullet+} + C_2. \qquad (17)$$

The critical energy was used as a parameter $5{\cdot}2\ eV \leqslant E_0 \leqslant 7{\cdot}1\ eV$. The calculations included radiative decay in the infrared with $k_{rad} = 100\ s^{-1}$. It was concluded that the resilience towards decomposition observed for $C_{60}^{\bullet+}$ by Whetten and co-workers [101] under surface-induced decomposition was due to the short time (of the order of microseconds) available. These calculations indicated that while, at $t = 1\ \mu s$, $C_{60}^{\bullet+}$ is intact even for a transferred energy of 40 eV, it is completely dissociated at $t = 1$ s. A large cross-over shift between 1 μs and 1 s was predicted (greater than 20 eV) and an intrinsic shift $IS \leqslant 20$ eV. These estimates were shown to be wrong (see section 3.4 and table 1) for one major reason: radiative decay in C_{60} is at least one order of magnitude faster than $10^2\ s^{-1}$, owing to emission in the visible via a black-body radiative cooling mechanism, demonstrated by Kolodney *et al.* [102] and Campbell and co-workers [103]. An IR radiative decay rate–energy dependence was calculated by Anderson and co-workers [104] on the basis of an empirical equation by Dunbar (figure 14). The value of $E_0 = 7{\cdot}1 \pm 0{\cdot}4$ eV first obtained from electron ionization experiments of Märk's group [80] is now fairly generally accepted as the correct value [106]. Inspection of figure 14, which we have reviewed earlier [79], demonstrates that the curve for k_{rad} cuts the dissociative $k(E)$ curve for reaction (17), provided that $E_0 = 7{\cdot}2$ eV, at an internal energy of about 40 eV and at a rate of about $10^3\ s^{-1}$. This calculation thus predicts that no dissociation should be observed below an internal energy of about

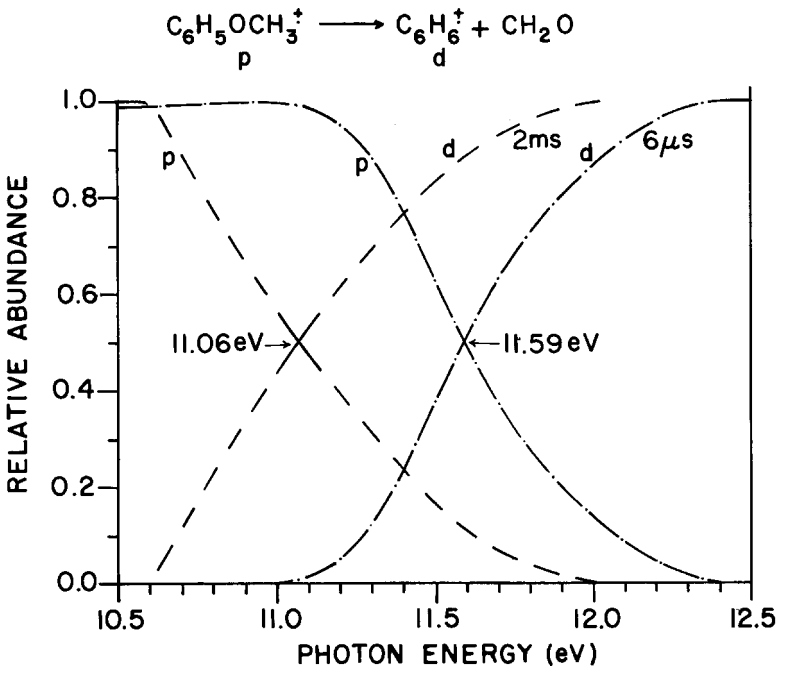

Figure 12. Experimental breakdown curves for anisole for 6 μs and 2 ms residence times [26].

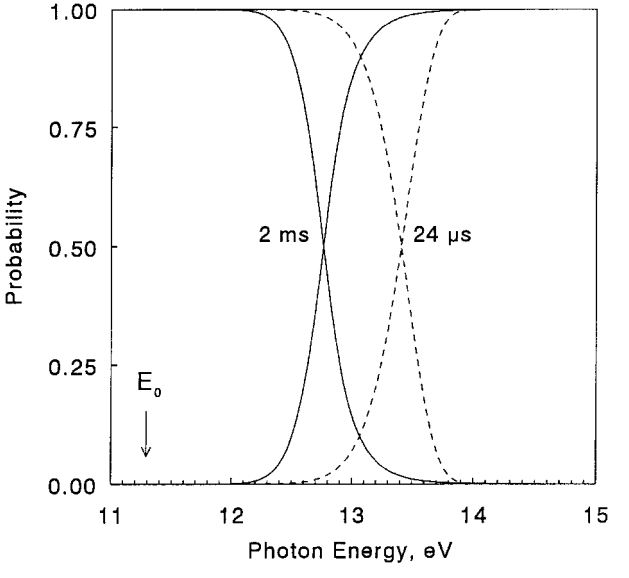

Figure 13. Calculated time-resolved 0 K breakdown curves for parent and daughter ions ($C_{10}H_7Br^{+\cdot}$ and $C_{10}H_7^+$ respectively) of 1-bromonaphthalene at the two indicated reaction times. The cross-over shift, which is the shift in cross-over energies (equal parent and daughter ion probabilities) between 24 μs and 2 ms, is calculated to be 0·71 eV [40].

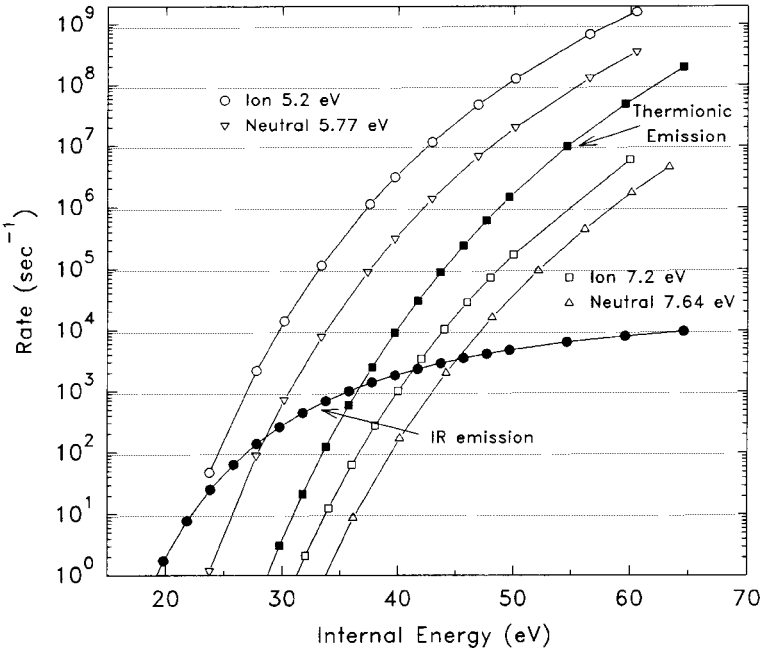

Figure 14. Calculated rates for C_2 loss, thermionic emission and IR emission for C_{60} and $C_{60}^{\bullet+}$. The low ion and neutral binding energies are from [105]; the high ion and neutral binding energies are from [80]. The infrared radiative decay of $C_{60}^{\bullet+}$ was calculated [104] on the basis of an empirical equation obtained by Dunbar.

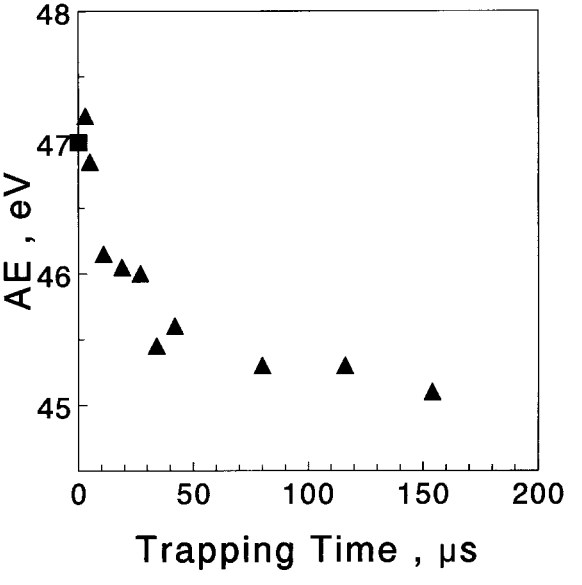

Figure 15. Time-resolved $C_{58}^{\bullet+}$ AE as a function of ion-trapping time at T = 620 K : (▲), Space-charge trapping; (■), without trapping, taken from [109] and corrected for the temperature difference [38].

40 eV contrary to our original predictions [100]. However, even the radiative decay curve (figure 14) may have to be modified, in view of the recent findings concerning black-body radiation in the visible [102, 103].

3.4. *Time-resolved appearance energies for fragment ions from* C_{60}

We have started the discussion of C_2 evaporation from C_{60} in section 3.3.3. The C_2 binding energy remains controversial; however, as noted earlier, the value $E_0 = 7{\cdot}1 \pm 0{\cdot}4$ eV is now preferred [80]. Two recent review articles in this journal, by Klots [106] and by Märk and co-workers [107], have addressed various aspects of reaction (17) including consecutive C_2 evaporations from $C_{58}^{\bullet+}$, $C_{56}^{\bullet+}$, etc. A reinvestigation of the kinetic energy release distribution (KERD) by Lifshitz and co-workers [81] led to $E_0 = 7{\cdot}1 \pm 0{\cdot}5$ eV instead of the original value of $E_0 = 5{\cdot}2$ eV [105]. This reconciles the KERD data with those derived from electron ionization breakdown curves, by Märk and co-workers [80]. A self-consistent determination of fullerene binding energies $BE(C_n^+–C_2)$, $n = 58, \ldots, 44$ followed [82], and an upper limit for the binding energy $BE(C_{58}^+–C_2) \approx 7{\cdot}6$ eV was estimated (table 2).

Time-resolved AEs for fragment ions from C_{60} were measured by electron ionization, using space-charge trapping in a VG ZAB-2F ion source at The Hebrew University and by Fourier transform ion cyclotron resonance at Argonne [38]. The ionization efficiency curve of Xe^{2+} was employed to calibrate the energy scales of the two experiments. C_{60} was evaporated at a temperature of 620 K. All the time-resolved electron ionization efficiency curves were treated by the method of Scheier *et al*. [108]. The individual data sets were modified by a power law in order to linearize the threshold region and linear regressions allowed the determination of AEs. The $C_{58}^{\bullet+}$ AEs obtained in this fashion are plotted as a function of trapping time in figure 15. A sharp drop at low trapping times and a levelling off at long times with a limiting value of AE = 45·1 eV was observed from the results of space charge trapping (figure 15). The AE obtained in a similar fashion from the Fourier transform mass spectrometry experiment at 120 ± 20 ms was AE = 44 ± 2 eV. These values are considerably higher than originally expected for an ion-trapping experiment unlimited by ion containment time [79]. The result is in line with the two more recent developments discussed above.

(*a*) The binding energy $BE(C_{58}^{\bullet+}–C_2)$ is now better established as $7{\cdot}1(\pm 0{\cdot}4)$ eV [80, 81] rather than the value of 5·2 eV [105] preferred in our earlier calculations [100].

(*b*) $C_{60}^{\bullet+}$ undergoes black-body-like radiative decay by analogy with C_{60} [102, 103] at a much faster rate (10^3 s^{-1} or greater) than the IR radiative decay of 10^2 s^{-1} originally assumed [100].

The AEs determined by the linearization procedure are affected by prior background subtraction. A lower limit on the long time AE obtained both by space-charge trapping and by FTICR was 42·0 eV [38].

The internal energy onset for C_2 loss can be calculated [38]:

$$\begin{aligned} E_{\text{int}} &= \text{AE} + \bar{E}(620\ \text{K}) - \text{IE} \\ &= 42{\cdot}0 + 3{\cdot}2 - 7{\cdot}6 = 37{\cdot}6\ \text{eV}, \end{aligned} \tag{18}$$

where $\bar{E}(620\ \text{K})$ is the average thermal energy of the vaporized neutral and IE is the first ionization energy of C_{60}. $E_{\text{int}} = 37{\cdot}6$ eV corresponds to a temperature of 2330 K. This temperature is the isokinetic bath temperature (equation (19) of [106]) calculated

Table 3. Selected ionic heats of formation.

Species	$\Delta_f H_0$ (kcal mol^{-1}) 0 K	298 K	Reference
$C_8H_6^{\bullet+}$ (benzocyclobutadiene?)	276 ± 5; 280·6 ± 1		[41, 42]
$C_{10}H_7^+$ (α-naphthyl)	281 ± 3		[40]
$C_{10}H_7Br^{\bullet+}$ (bromonaphthalene)	235		[40]
$C_{11}H_9^+$ (benzotropylium?)		⩽ 213 ± 5	[43]
$C_{11}H_{10}^{\bullet+}$ (1-methylnaphthalene)		209·3 ± 1	[43]
$C_{14}H_8^{\bullet+}$ (dehydroanthracene)	⩽ 297 + 3		[63]
$C_{14}H_9^+$ (anthracenyl)	289 ± 3		[63]
$C_{14}H_9Br^{\bullet+}$ (bromoanthracene)	241		[63]
$C_{16}H_9^+$ (pyrenyl)	284		[44]
$C_{16}H_9^+$ (fluoranthenyl)	308		[45]
$C_{16}H_{10}^{\bullet+}$ (pyrene)	230		[44]
$C_{16}H_{10}^{\bullet+}$ (fluoranthene)	258		[45]

via equation (A 5) of [110]. In other words, the experimental results of Laskin *et al.* [38] show that C_2 loss from $C_{60}^{\bullet+}$ occurs at $T > 2300$ K and black-body radiative decay below 2300 K.

The IS is given by [38] (table 1)

$$\text{IS} = E_{\text{int}} - E_0 = 37{\cdot}6 - 7{\cdot}1 = 30{\cdot}5 \text{ eV}. \tag{19}$$

Thus, while the resilience of $C_{60}^{\bullet+}$ towards decomposition is time dependent as predicted [100], the time range and energy regime over which the changes in AE take place are much more limited than originally anticipated (see figure 15).

3.5. *Bond energies and heats of formation*

The critical energies E_0 for reactions proceeding via loose transition states ($\Delta S^{\ddagger} > 0$) have been equated with the endothermicities of the reactions, since such reactions do not possess reverse activation energies. This has allowed us to deduce some new bond energies and heats of formation. The values to which we ascribe the greatest certainty are the C–H bond energy in naphthalene$^{\bullet+}$ and the heat of the formation of the α-napthyl cation, and their derivation will be described in greater detail here. These values and others, derived in the course of our recent studies, are summarized in tables 3 and 4. Values derived for phenanthrene [42] are not included, since that part of our work is now being repeated [85].

The critical energy of activation for reaction (8) [40] is $E_0 = 3{\cdot}23 \pm 0{\cdot}07$ eV. The heat of formation of 1-bromonaphthalene has been estimated [1] from group contributions to be $\Delta_f H^0_{298\text{ K}}(C_{10}H_7Br) = 42$ kcal mol^{-1}. The heat of formation at 0 K was calculated [40] from the room-temperature value and from the frequencies [111], using standard statistical mechanics methods: $\Delta_f H^0_0(C_{10}H_7Br) = 48{\cdot}4$ kcal mol^{-1}. Employing the ionization energy of 1-bromonaphthalene [40], $IE(C_{10}H_7Br) = 8{\cdot}08 \pm 0{\cdot}03$ eV gives $\Delta_f H^0_0(C_{10}H_7Br^{\bullet+}) = 235$ kcal mol^{-1}. Since $\Delta_f H^0_0(Br^{\bullet}) = 28{\cdot}2$ kcal mol^{-1} [1], the heat of formation of the α-napthyl cation is calculated [40] to be $\Delta_f H^0_0(C_{10}H_7^+) = 281$ kcal mol^{-1}. The greatest uncertainty in the $\Delta_f H^0_0(C_{10}H_7^+)$ value comes from the uncertainty in the heat of formation of the neutral precursor and has been estimated to be ± 3 kcal mol^{-1} [40].

Table 4. Selected bond energies (eV) for PAH ions and bromime substituted PAH ions.

Compound	Bond	Bond energy (eV)	Reference
Benzene	$C_6H_5^+$–$H^{\bullet}$	3·61 ± 0·13	[15]
		3·88	[36]
Naphthalene	$C_{10}H_7^+$–$H^{\bullet}$	4·48 ± 0·10	[41]
Anthracene	$C_{14}H_9^+$–$H^{\bullet}$	4·67	[63]
Pyrene	$C_{16}H_9^+$–$H^{\bullet}$	4·60	[44]
Bromobenzene	$C_6H_5^+$–$Br^{\bullet}$	2·76	[22]
Bromonaphthalene	$C_{10}H_7^+$–$Br^{\bullet}$	3·23	[40]
Bromoanthracene	$C_{14}H_9^+$–$Br^{\bullet}$	3·30	[63]
Toluene	$C_7H_7^+$–$H^{\bullet}$	2·11	[62]
Methylnaphthalene	$C_{11}H_9^+$–$H^{\bullet}$	2·41	[43]

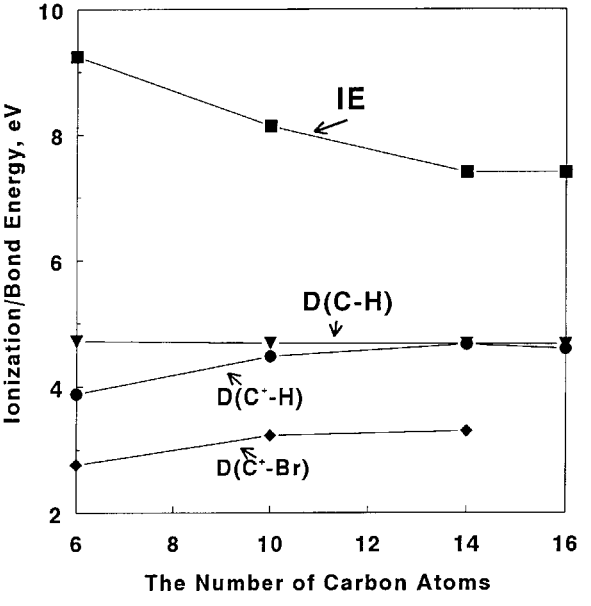

Figure 16. IEs (■) of PAHs (benzene, naphthalene, anthracene and pyrene); C–H bond energies of PAH neutrals (▼) and cations (●) and C–Br bond energies (◆) of bromine substituted PAH cations as a function of the number of carbon atoms [63].

The C–H bond energy of the naphthalene radical cation may be calculated [40, 41] from the heat of formation of α-napthyl cation, $\Delta_f H_0^0(C_{10}H_7^+) = 281 \pm 3$ kcal mol^{-1} [40], and from the known heats of formation [1], $\Delta_f H_0^0(C_{10}H_8^{\bullet+}) = 229{\cdot}2$ kcal mol^{-1} for the naphthalene radical cation and $\Delta_f H_0^0(H^{\bullet}) = 51{\cdot}63$ kcal mol^{-1}, $D(C_{10}H_7^+$–$H^{\bullet}) = 4{\cdot}48$ eV [41]. This calculated value is exactly equal to the critical energy obtained for reaction (14) by Ho *et al.* [41], $E_0 = 4{\cdot}48 \pm 0{\cdot}10$ eV.

Gotkis *et al.* [40] noticed that there was a consistent increase in analogous bond energies on going from benzene to naphthalene ion derivatives. This holds for the C–H bond energies in $C_6H_6^{\bullet+}$ as against $C_{10}H_8^{\bullet+}$, the C–H bond energies in $C_7H_8^{\bullet+}$ as against $C_{11}H_{10}^{\bullet+}$ and in $C_6H_5Br^{\bullet+}$ as against $C_{10}H_7Br^{\bullet+}$. This trend has been studied further for larger ring systems, and some of the results are included in table 4 and represented graphically in figure 16 [63]. The C–H bond energies for neutral PAHs are taken from [112]. These are almost independent of the ring system size. The C–H bond energy of

ionic PAHs increases from benzene to naphthalene, but the further increase from naphthalene to anthracene is small. It seems that the bond weakening upon ionization becomes negligible for anthracene and pyrene and the C–H bond energies of ionic PAHs approach those of the neutral PAHs with increasing size.

4. Conclusion

We have described experiments and theoretical modelling for evaluating the kinetic shift by measuring the shift of the fragment ionization efficiency curve along the energy axis as the residence time of the ion is varied, an idea put forward by Chupka and Berkowitz [5]. This was demonstrated to be very successful for cases such as the $Br^{\bullet}$ loss from $C_6H_5Br^{\bullet+}$ [22] for which the IS due to competition between dissociative and radiative decay is negligibly small (0·07 eV or less). For the larger molecules discussed here, that is PAHs and fullerenes, the situation becomes much more complex. The IS becomes an increasingly larger fraction of the total kinetic shift with increasing molecular size (table 1). Elaborate kinetic modelling is required, in order to gain information concerning the energetics and dynamics of the unimolecular dissociations of these large ionic species. Combining TPIMS measurements with TRPD data for the same species has been very valuable in pinning down rate–energy dependences, even if only a single value or at most two $k(E)$ values could be determined by TRPD in the $k(E)$ range of approximately 10^2–10^4 s^{-1}. The kinetic modelling required to derive activation parameters, bond energies and heats of formation involves, as it has in the past, statistical theories such as RRKM QET or microcanonical variational transition state theory. However, in addition, modelling of the radiative decay is an essential requirement. That can be done for IR radiative decay of the PAHs in a fairly accurate way [96–99]. The results presented here for bromonaphthalene and for naphthalene, which have combined TPIMS with TRPD data [40, 41] are considered to be particularly accurate and the bond dissociation energy $C_{10}H_7^+$–$H^{\bullet}$ in naphthalene is probably better established than for the corresponding neutral. The full understanding and correct modelling of radiative decay and its competition with dissociative decay in C_{60} and other fullerenes may still require further work. Whether other large species undergo radiative cooling by black-body-like emission in the visible remains an open question.

Acknowledgments

This work was supported by a grant from the German–Israeli Foundation for Scientific Research and Development and by the Israel Science Foundation. Earlier work described in this review article was supported by the Basic Research Foundation administered by the Israel Academy of Science and Humanities, by the Israeli Ministry of Absorption and Ministry of Science and Development, by the US–Israel Binational Science Foundation and by a Max Planck Research Award.

I would like to thank all my students and co-workers without whom the work described here could not have been accomplished. Special thanks are due to Professor R. C. Dunbar and his students at Case Western Reserve University for the TRPD measurements, which were crucial for the understanding and modelling of the larger molecules discussed in this review.

References

[1] Lias, S. G., Bartmess, J. E., Liebman, J. F., Holmes, J. L., Levin, R. D., and Mallard, W. G., 1988, *J. phys. Chem. Ref. Data*, **17**, Suppl. 1.
[2] Friedman, L., Long, F. A., and Wolfsberg, M. 1957, *J. chem. Phys.*, **26**, 714.
[3] Chupka, W. A., 1959, *J. chem. Phys.*, **30**, 191.
[4] Lifshitz, C., 1982, *Mass Spectrom. Rev.*, **1**, 309.
[5] Chupka, W. A., and Berkowitz, J., 1960, *J. chem. Phys.*, **32**, 1546.
[6] Lifshitz, C., MacKenzie Peers, A., Weiss, M., and Weiss, M. J., 1974, *Adv. Mass. Spectrom.*, **6**, 871.
[7] Lifshitz, C., Weiss, M., and Landau-Gefen, S. *25th Annual Conference on Mass Spectrometry and Allied Topics, Abstracts* Washington, DC, June 1977 (American Society for Mass Spectrometry), pp. 512–514.
[8] Lifshitz, C., and Gefen, S., 1980, *Int. J. Mass Spectrom. Ion Phys.*, **35**, 31.
[9] Lifshitz, C., 1982, *J. phys. Chem.*, **86**, 606.
[10] Lifshitz, C., Gotchiguian, P., and Roller, R., 1983, *Chem. Phys. Lett.*, **95**, 106.
[11] Lifshitz, C., and Eaton, P., 1983, *Int. J. Mass Spectrom. Ion Phys.*, **49**, 337.
[12] Lifshitz, C., Goldenberg, M., Malinovich, Y., and Peres, M., 1983, *Int. J. Mass Spectrom. Ion Phys.*, **46**, 269.
[13] Lifshitz, C., and Gefen, S., 1984, *Org. Mass Spectrom.*, **19**, 197.
[14] Gefen, S., and Lifshitz, C., 1984, *Int. J. Mass Spectrom. Ion Processes*, **58**, 251.
[15] Davico, G. E., Bierbaum, V. M., DePuy, C. H., Ellison, G. B., and Squires, R. R., 1995, *J. Am. chem. Soc.*, **117**, 2590.
[16] Butcher, V., Costa, M. L., Dyke, J. M., Ellis, A. R., and Morris, J. A., 1987, *Chem. Phys. Lett.*, **115**, 261.
[17] Burgers, P. C., Holmes, J. L., Mommers, A. A., and Terlouw, J. K., 1983, *Chem. Phys. Lett.*, **102**, 1.
[18] Chupka, W. A., and Kaminsky, M., 1961, *J. chem. Phys.*, **35**, 1991.
[19] Lifshitz, C., Goldenberg, M., Malinovich, Y., and Peres, M., 1982, *Org. Mass Spectrom.*, **17**, 453.
[20] Lifshitz, C., 1991, *Int. J. Mass Spectrom. Ion Processes*, **106**, 159.
[21] Lifshitz, C., and Malinovich, Y., 1984, *Int. J. Mass Spectrom. Ion Processes*, **60**, 99.
[22] Malinovich, Y., Arakawa, R., Haase, G., and Lifshitz, C., 1985, *J. phys. Chem.*, **89**, 2253.
[23] Malinovich, Y., and Lifshitz, C., 1986, *J. phys. Chem.*, **90**, 2200.
[24] Malinovich, Y., and Lifshitz, C., 1986, *J. phys. Chem.*, **90**, 4311.
[25] Ziesel, J. P., Malinovich, Y., Ohmichi, N., and Lifshitz, C., 1987, *Chem. Phys. Lett.*, **136**, 81.
[26] Ziesel, J. P., and Lifshitz, C., 1987, *Chem. Phys.*, **117**, 227.
[27] Ohmichi, N., Malinovich, Y., Ziesel, J. P., and Lifshitz, C., 1989, *J. phys. Chem.*, **93**, 2491.
[28] Lifshitz, C., and Ohmichi, N., 1989, *J. phys. Chem.*, **93**, 6329.
[29] Faulk, J. D., Dunbar, R. C., and Lifshitz, C., 1990, *J. Am. chem. Soc.*, **112**, 7893.
[30] Ohmichi, N., Gotkis, I., Steens, L., and Lifshitz, C., 1992, *Org. Mass Spectrom.*, **27**, 383.
[31] Lifshitz, C., Gotkis, Y., Ioffe, A., Laskin, J., and Shaik, S., 1993, *Int. J. Mass Spectrom. Ion Processes*, **125**, R7.
[32] Lifshitz, C., Gotkis, Y., Laskin, J., Ioffe, A., and Shaik, S., 1993, *J. phys. Chem.*, **97**, 12291.
[33] Lifshitz, C., 1994, *Accts Chem. Res.*, **27**, 138.
[34] Lifshitz, C., Levin, I., Kababia, S., and Dunbar, R. C., 1991, *J. phys. Chem.*, **95**, 1667.
[35] Lifshitz, C., Louage, F., Aviyente, V., and Song, K., 1991, *J. phys. Chem.*, **95**, 9298.
[36] Klippenstein, S. J., Faulk, J., and Dunbar, R. C., 1993, *J. chem. Phys.*, **98**, 243.
[37] Huang, F.-S., and Dunbar, R. C., 1990, *J. Am. chem. Soc.*, **112**, 8167.
[38] Laskin, J., Behm, J. M., Lykke, K. R., and Lifshitz, C., 1996, *Chem. Phys. Lett.*, **252**, 277.
[39] Dunbar, R. C., and Lifshitz, C., 1991, *J. chem. Phys.*, **94**, 3542.
[40] Gotkis, Y., Naor, M., Laskin, J., Lifshitz, C., Faulk, J. D., and Dunbar, R. C., 1993, *J. Am. chem. Soc.*, **115**, 7402.
[41] Ho, Y.-P., Dunbar, R. C., and Lifshitz, C., 1995, *J. Am. chem. Soc.*, **117**, 6504.
[42] Gotkis, Y., Oleinikova, M., Naor, M., and Lifshitz, C., 1993, *J. phys. Chem.*, **97**, 12282.

[43] Gotkis, I., and Lifshitz, C., 1993, *Org. Mass Spectrom.*, **28**, 372.
[44] Ling, Y., Gotkis, Y., and Lifshitz, C., 1995, *Eur. Mass Spectrom.*, **1**, 41.
[45] Ling, Y., and Lifshitz, C., 1995, *J. Phys. Chem.*, **99**, 11074.
[46] March, R. E., and Hughes, R. J., 1989, *Quadrupole Storage Mass Spectrometry* (New York: Wiley), p. 308.
[47] Mather, R. E., Waldren, R. M., Todd, J. F. J., and March, R. E., 1980, *Int. J. Mass Spectrom. Ion Phys.*, **33**, 201.
[48] Lifshitz, C., Nadav, E., Peres, M., Peres, T., Laskin, J., Karsenty, B., and Shaked, M., 1994, *Int. J. Mass Spectrom. Ion Processes*, **133**, L11.
[49] Morgan, R. P., Beynon, J. H., Bateman, R. H., and Green, B. N., 1978, *Int. J. Mass Spectrom. Ion Phys.*, **28**, 171.
[50] Kirchner, N. J., and Bowers, M. T., 1987, *J. phys. Chem.*, **91**, 2573.
[51] Hasted, J. B., 1967, *Some Newer Methods in Structural Chemistry*, edited by R. Bonnett and J. G. Davis (London: United Trade Press); Baker, F. A., and Hasted, J. B., 1966, *Phils. Trans. R. Soc.* A **261**, 33.
[52] Redhead, P. A., 1967, *Can. J. Phys.*, **45**, 1791.
[53] Herod, A. A., and Harrison, A. G., 1970, *Int. J. Mass Spectrom. Ion Phys.*, **4**, 415.
[54] Ryan, K. R., and Graham, I. G., 1973, *J. chem. Phys.*, **59**, 4260; Ryan, K. R., 1974, *J. chem. Phys.*, **61**, 1559.
[55] Lifshitz, C., and Weiss, M., 1980, *Int. J. Mass Spectrom. Ion Phys.*, **34**, 311.
[56] Koppel, C., Schwarz, H., and Bohlmann, F., 1974, *Org. Mass Spectrom.*, **8**, 25.
[57] Nounou, P., 1966, *J. Chim. phys.*, **65**, 994.
[58] Loudon, A. G., and Mazengo, R. Z., 1974, *Org. Mass. Spectrom.*, **8**, 179.
[59] Hase, W. L., and Bunker, D. L., *Quantum Chemistry Program Exchange*, No. 234 (Chemistry Department, Indiana University).
[60] Chupka, W. A., and Berkowitz, J., 1967, *J. chem. Phys.*, **47**, 2921.
[61] Lifshitz, C., 1989, *Adv. Mass Spectrom.*, **11**, 713.
[62] Huang F.-S., and Dunbar, R. C., 1991, *Int. J. Mass Spectrom. Ion Processes*, **109**, 151.
[63] Ling, Y., Martin, J. M. L., and Lifshitz, C., 1996, *Int. J. Mass Spectrom. Ion Processes* (to be published).
[64] Pachuta, S. J., Kenttämaa, H. I., Sack, T. M., Cerny, R. L., Tomer, K. B., Gross, M. L., Pachuta, R. R., and Cooks, R. G., 1988, *J. Am. chem. Soc.*, **110**, 657.
[65] Baer, T., Sai, B. P., Smith, D., and Murray, P. T., 1976, *J. chem. Phys.*, **64**, 2460.
[66] Rosenstock, H. M., Stockbauer, R., and Parr, A. C., 1980, *J. chem. Phys.*, **73**, 773.
[67] Dunbar, R. C., and Honovich, J. P., 1984, *Int. J. Mass Spectrom. Ion Processes*, **58**, 25.
[68] Neusser, H. J., 1989, *J. phys. Chem.*, **93**, 3897.
[69] Rühl, E., Price, S. D., and Leach, S., 1989, *J. phys. Chem.*, **93**, 6312.
[70] Rosentock, H. M., Stockbauer, R., and Parr, A. C., 1979, *J. chem. Phys.*, **71**, 3708.
[71] Dannacher, J., Rosenstock, H. M., Buff, R., Parr, A. C., Stockbauer, R. L., Bombach, R., and Stadelman, J.-P., 1983, *Chem. Phys.*, **75**, 23.
[72] Pratt, S. T., and Chupka, W. A., 1981, *Chem. Phys.*, **62**, 153.
[73] Dunbar, R. C., 1987, *J. phys. Chem.*, **91,** 2801.
[74] So, H. Y., and Dunbar, R. C., 1988, *J. Am. chem. Soc.*, **110**, 3080.
[75] Dunbar, R. C., 1989, *J. chem. Phys.*, **91**, 6080.
[76] Dunbar, R. C., 1990, *J. phys. Chem.*, **94**, 3283.
[77] Dunbar, R. C., 1991, *J. chem. Phys.*, **94**, 3542.
[78] Kühlewind, H., Kiermeier, A., and Neusser, H. J., 1986, *J. chem. Phys.*, **85**, 4427.
[79] Lifshitz, C., 1993, *Mass Spectrom. Rev.*, **12**, 261.
[80] Foltin, M., Lezius, M., Scheier, P., and Märk, T. D., 1993, *J. chem. Phys.*, **98**, 9624.
[81] Laskin, J., Jimenez-Vazquez, H. A., Shimshi, R., Saunders, M., de Vries, M. S., and Lifshitz, C., 1995, *Chem. Phys. Lett.*, **242**, 249.
[82] Wörgötter, R., Dünser, B., Scheier, P., Märk, T. D., Foltin, M., Klots, C. E., Laskin, J., and Lifshitz, C., 1996, *J. chem. Phys.*, **104**, 1225.
[83] Werner, A. S., and Baer, T., 1975, *J. chem. Phys.*, **62**, 2900.
[84] Baer, T., 1979, *J. Electron Spectrosc. relat. Phenom.*, **15**, 225.
[85] Ling, Y., and Lifshitz, C., 1997 (to be published).
[86] Olesik, S., Baer, T., Morrow, J. C., Ridal, J. J., Buschek, J., and Holmes, J. L., 1989, *Org. Mass Spectrom.*, **24**, 1008.
[87] Lin, C. Y., and Dunbar, R. C., 1994, *J. phys. Chem.*, **98**, 1369.

[88] JOCHIMS, H. W., RASEKH, H., RÜHL, E., BAUMGÄRTEL, H., and LEACH, S., 1992, *Chem. Phys.*, **168**, 159.
[89] JOCHIMS, H. W., RASEKH, H., RÜHL, E., BAUMGÄRTEL, H., and LEACH, S., 1993, *J. phys. Chem.*, **97**, 1312.
[90] GRANUCCI, G., ELLINGER, Y., and BOISSEL, P., 1995, *Chem. Phys.*, **191**, 165.
[91] LING, Y., MARTIN, J. M. L., and LIFSHITZ, C., 1997, *J. phys. Chem.* A, **101**, 219.
[92] STOCKBAUER, R., and ROSENSTOCK, H. M., 1978, *Int. J. Mass Spectrom Ion Phys.*, **27**, 185.
[93] ROSENSTOCK, H. M., STOCKBAUER, R., and PARR, A. C., 1981, *Int. J. Mass Spectrom. Ion Phys.*, **38**, 323.
[94] ROSENSTOCK, H. M., STOCKBAUER, R., and PARR, A. C., 1980, *J. Chim. phys.*, **77**, 745.
[95] DUNBAR, R. C., 1975, *Spectrochim. Acta* A, **31**, 797.
[96] KIM, M. S., and DUNBAR, R. C., 1980, *J. chem. Phys.*, **72**, 4405.
[97] DUNBAR, R. C., CHEN, J. H., SO, H. Y., and ASAMOTO, B., 1987, *J. chem. Phys.*, **86**, 2081.
[98] DUNBAR, R. C., 1992, *Mass Spectrom. Rev.*, **11**, 309.
[99] HO, Y.-P., YANG, Y.-C., KLIPPENSTEIN, S. J., and DUNBAR, R. C., 1995, *J. phys. Chem.*, **99**, 12115.
[100] LIFSHITZ, C., GOTKIS, I., SANDLER, P., and LASKIN, J., 1992, *Chem. Phys. Lett.*, **200**, 406; GOTKIS, Y., LASKIN, J., and LIFSHITZ, C., 1993, *Proceedings of the 41st ASMS Conference on Mass Spectrometry and Allied Topics*, San Francisco, California, 1993.
[101] BECK, R. C., ST. JOHN, P., ALVAREZ, M. M., DIEDERICH, F., and WHETTEN, R. L., 1991, *J. Phys. Chem.*, **95**, 8402.
[102] KOLODNEY, E., BUDREVICH, A., and TSIPINYUK, B., 1995, *Phys. Rev. Lett.*, **74**, 510.
[103] MITZNER, R., and CAMPBELL, E. E. B., 1995, *J. chem. Phys.*, **103**, 2445.
[104] WAN, Z., CHRISTIAN, J. F., BASIR, Y., and ANDERSON, S. L., 1993, *J. chem. Phys.*, **99**, 5858.
[105] SANDLER, P., LIFSHITZ, C., and KLOTS, C. E., 1992, *Chem. Phys. Lett.*, **200**, 445.
[106] KLOTS, C. E., 1996, *Int. Rev. phys. Chem.*, **15**, 205.
[107] SCHEIER, P., DÜNSER, B., WÖRGÖTTER, R., MATT, S., MUIGG, D., SENN, G., and MÄRK, T. D., 1996, *Int. Rev. phys. Chem.*, **15**, 93.
[108] SCHEIER, P., DÜNSER, B., WÖRGÖTTER, R., LEZIUS, M., ROBL, R., and MÄRK, T. D., 1994, *Int. J. Mass Spectrom. Ion Processes*, **138**, 77.
[109] WÖRGÖTTER, R., DÜNSER, B., SCHEIER, P., and MÄRK, T. D., 1994, *J. chem. Phys.*, **101**, 8674.
[110] KLOTS, C. E., 1989, *Phys. Rev.* A, **39**, 339.
[111] SINGH, S. N., BHATT, H. S., and SINGH, R. D., 1978, *Spectrochim. Acta*, **34**, 985.
[112] CHEN, R. H., KAFAFI, S. A., and STEIN, S. E., 1989, *J. Am. Chem. Soc.*, **111**, 1418.